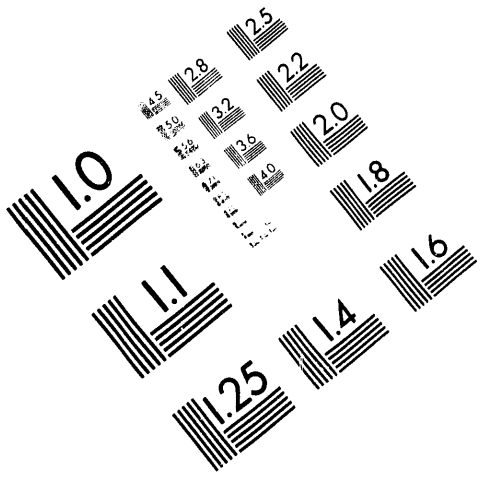

Association for Information and Image Management

1100 Wayne Avenue, Suite 1100
Silver Spring, Maryland 20910

301/587-8202

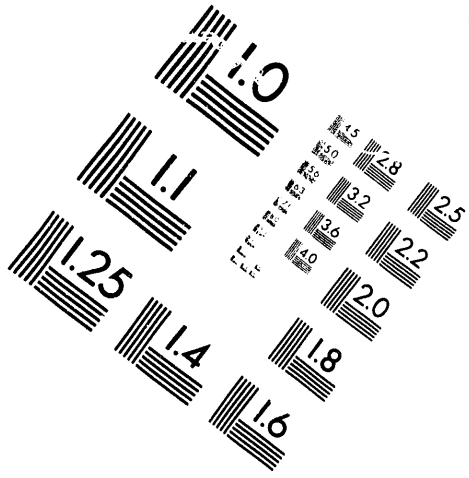

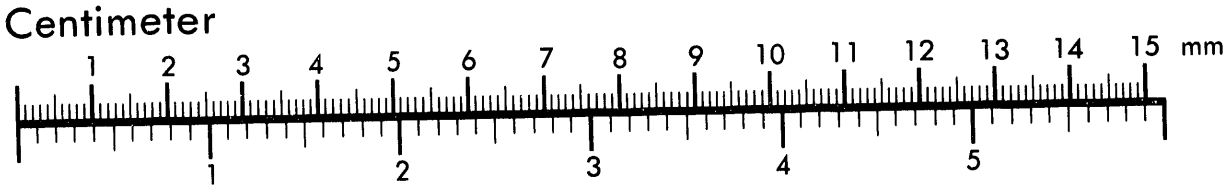

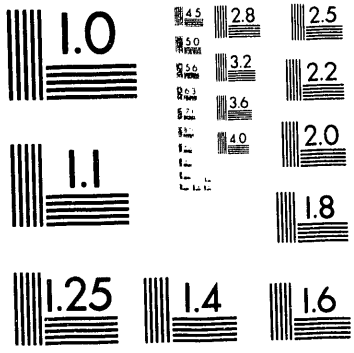

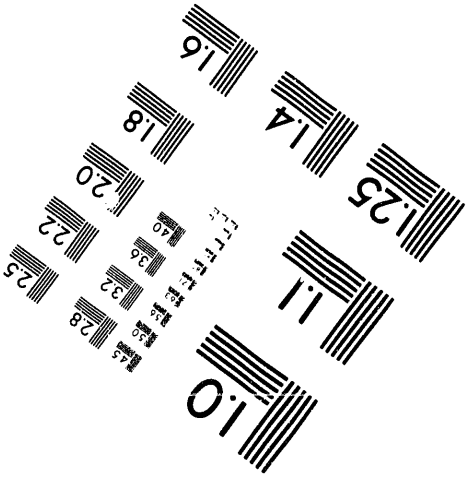

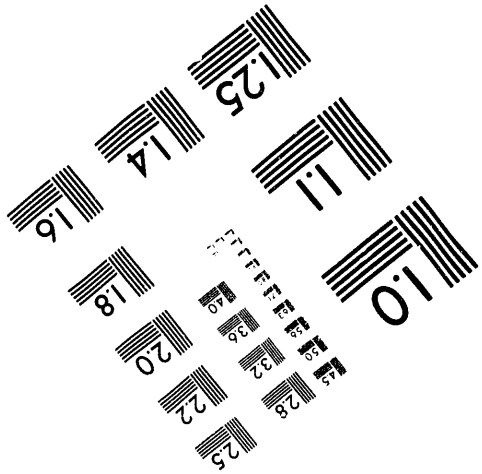

1 of 1

2

Conf-9305100--1

PNL-SA-21622

LOW-TEMPERATURE SINTERING AND PHASE CHANGES IN CHROMITE INTERCONNECT MATERIALS

L. A. Chick
D. E. McCready
G. D. Maupin
T. R. Armstrong
G. W. Coffey
J. L. Bates

May 1993

Presented at the
Third Industrial Symposium on
Solid Oxide Fuel Cells
May 16-21, 1993
Honolulu, Hawaii

Prepared for
the U.S. Department of Energy
Contract DE-AC06-76RLO 1830

Pacific Northwest Laboratory
Richland, Washington 99352

LOW-TEMPERATURE SINTERING AND PHASE CHANGES IN CHROMITE INTERCONNECT MATERIALS

L. A. Chick, T. R. Armstrong, D. E. McCready,
G. W. Coffey, G.D. Maupin and J. L. Bates
Pacific Northwest Laboratory*
PO Box 999
Richland, Washington 99352

ABSTRACT

Sintering shrinkage curves and phase changes were compared for calcium-substituted lanthanum chromites with either slight A-site enrichment or depletion. Of the former type, $La_{0.7}Ca_{0.31}CrO_3$ that was synthesized by the glycine-nitrate method sintered to high density in air at 1250°C, exhibiting two rapid-shrinkage events. Weight loss measurements corroborated XRD data showing that, prior to densification, over half the Ca resided in non-perovskite phases, including $CaCrO_4$. In the $La_{0.7}Ca_{0.31}CrO_3$, densification was closely associated with re-dissolution of the Ca into the perovskite.

1. INTRODUCTION

The current interconnect in solid oxide fuel cells (SOFC) must be stable in both oxidizing and reducing environments near 1000°C, must have high electronic and low ionic conductivity, and must have a thermal expansion curve close to that of the electrolyte, yttria-stabilized zirconia. These combined requirements eliminate all but a few metals and ceramics. Several types of ABO_3 chromites, including $Y(Ca)CrO_3$ and $La(M)CrO_3$, where M is Mg, Ca, or Sr, have been developed that meet these requirements. However, these materials generally pose problems during SOFC fabrication.

The interconnect must be sintered to high density so that it will provide a gas-tight seal between the electrodes. Furthermore, decreasing the cost of SOFC manufacturing to the point that the technology is economically competitive may require that the several ceramic components are sintered together in one step. In order to prevent decomposition of the manganite cathode, such co-sintering would have to be performed in air at temperatures near or below 1400°C, conditions that are not favorable to chromite densification. For these reasons, a substantial effort has been devoted to developing air-sinterable chromites. Yokokawa et al presented a summary of the pertinent literature up to about 1990 [1].

*Operated for the US Department of Energy by Battelle Memorial Institute under contract DE-AC06-76RLO 1830.

Recently, it has been shown that chromite densification can be substantially improved by slightly enriching the overall concentration of A-site cations (La or Y and M) relative to B-site cations (mainly Cr) [1-12]. The main objective of this paper is to clarify the differences in phase changes and sintering between A-site enriched and A-site depleted chromites. Another purpose is to establish that the chromite powder synthesis method remains an important variable affecting sinterability.

2. EXPERIMENTAL

Chromite powders were synthesized by the glycine-nitrate technique, using a stoichiometric fuel/oxidant ratio [13,14]. Variations in the precursor solution heating process have been found to affect chromite sintering behavior. For the materials discussed in this paper, the solutions were prepared at approximately one molar concentration based on the perovskite, and were not heated prior to the batch-wise combustion step. Aliquots for 0.04 moles of chromite were placed in 5 liter stainless-steel beakers covered with 60 mesh screens and heated rapidly on a hot plate. Unless otherwise specified, all powders were calcined for 0.5 hr in air at 650°C and uniaxially pressed at 35 MPa followed by isostatic pressing at 140 MPa, producing pellets between 35 and 40% of theoretical density. Sintering was performed using 20mm diam. by 4mm thick pellets, placed on edge in an electric resistance furnace in air. Sintering shrinkage curves were measured in a vertical pushrod dilatometer with a 25g load on 6mm x 6mm cylindrical pellets. X-ray diffraction (XRD) was performed using a wide-range goniometer-based powder diffractometer with a fixed-anode Cu tube operated at 40kV, 45mA. XRD specimens were ground in agate to pass 325 mesh (44μm) and mixed with 20 wt% NIST Si as an internal standard.

3. RESULTS

Figure 1 shows the magnitude of the effect that slight variations in A/B cation ratio have on sintered density. This is a plot of percent of theoretical density attained by samples that were heated at 1.6°C/min and quenched. The samples with (La+Ca)/Cr<1.0, x=0.28 and 0.29, never attained 60% density, even by 1550°C. In contrast, the samples with A/B>1.0, x=0.31 and 0.32, attained densities over 90% by 1400°C.

As shown in Figure 2, the sintering shrinkage curves for $La_{0.7}Ca_{0.29}CrO_3$ (LCC29) and $La_{0.7}Ca_{0.31}CrO_3$ (LCC31) heated at 2°C/min, both exhibit periods of rapid shrinkage. However, there are two characteristic differences between these curves; the first rapid-shrinkage event starts almost 100°C lower in LCC31 than in LCC29 (about 950°C versus about 1040°C). Also, LCC31 exhibits a second rapid-shrinkage event, starting near 1150°C, that takes the sample to near full density by 1300°C. This second event appears as only a very slight dip in the curve for LCC29. These characteristic differences are reproducible, as shown in

Figure 3, which includes three complete replications for each composition. New powder was synthesized for each run. Much of the variability between curves for the same composition is due to variation in the sample distortion that is caused by vertical loading in the dilatometer. The same characteristic differences are exhibited between chromium-enriched and chromium-depleted compositions in the $Y(Ca)CrO_3$ system, as shown in Figure 4.

In order to investigate the phase changes associated with the rapid-shrinkage events, a series of quenched samples was prepared. These samples were heated at 2°C/min, then air quenched from various peak temperatures. The shrinkage results are plotted along with the dilatometer data in Figure 5, in which the triangles represent linear sintering shrinkages calculated from immersion density data. The magnitude of the shrinkages calculated for the quenched pellets is less than that measured by the dilatometer due to the loading-induced distortion of the dilatometer samples, discussed above. However, the quenched pellet data exhibit the same characteristic differences in the rapid-shrinkage events as do the dilatometer curves.

Results of XRD analyses on the quenched pellets are listed in Tables 1 and 2. The fraction of Ca in the perovskite phase was estimated from the perovskite orthorhombic unit cell volume, which was determined from XRD. Figure 6 is a plot of the relation between unit cell volume and Ca content. The bold curve was calculated from data published by Berjoan et al [15], whereas the three points were determined from XRD of samples heated at 10°C/min to 1500°C and held for 2 hours. The data in Tables 1 and 2 were determined from the (thin) line drawn through the points. In addition to the perovskite phase, samples quenched from temperatures up to 1126°C were found to contain $CaCrO_4$. The concentration of $CaCrO_4$ in each sample was estimated based on comparison of major peak intensities. The LCC29 sample that was quenched from 1067°C also contained approximately 0.5 wt% of β-$CaCr_2O_4$. No additional crystalline phases were detected in any of the other samples, however, the presence and quantity of X-ray amorphous material was inferred by performing a material balance to account for the total amounts of cations introduced during synthesis. This X-ray amorphous material, which was present in all samples up through 1126°C, may consist of poorly crystallized phases or the glassy remnants of liquid phases. The material balance calculations indicated that the X-ray amorphous material in LCC31 samples had slightly more Ca than Cr, with the atom ratio, Ca/Cr=0.53/0.47. The corresponding ratio for the LCC29 samples was Ca/Cr=0.48/0.52.

These XRD results clearly establish that over half of the Ca resides in non-perovskite phases at the onset of sintering (926°C). As discussed below, although the glycine-nitrate synthesized chromites are composed of a single perovskite phase after combustion, much of the Ca is exsoluted from the perovskite during calcination, forming the $CaCrO_4$ and other minor phases. This exsoluted Ca, along with the associated Cr, dissolves back into the perovskite phase during sintering. In Figure 7, the Ca concentrations determined for the perovskite phase are plotted along with the dilatometer shrinkage curves. This plot shows that, for

both samples, dissolution of the Ca into the perovskite proceeds at roughly constant rate up to 1126°C, then more rapidly proceeds to completion at 1207°C. The more rapid dissolution is concurrent with the second rapid-shrinkage event in LCC31. Thus, although both materials experience rapid dissolution of Ca in this temperature interval, only LCC31 exhibits rapid densification.

Table 1. Results of XRD analyses of $La_{0.7}Ca_{0.29}CrO_3$ samples heated at 2°C/min in air to peak temperature, then quenched.

Peak Temp.°C	Ca Concentration in Perovskite Phase (x)	Mole Fraction $La_{1-x}Ca_xCrO_3$ Phase	Mole Fraction $CaCrO_4$ Phase	Mole Frac. X-Ray Amorphous Phase
800	0.07	0.75	0.13	0.12
926	0.12	0.79	0.11	0.10
1015	0.15	0.83	0.09	0.09
1067	0.17	0.85	0.04	0.11
1126	0.17	0.86	0.03	0.12*
1207	0.30	1.00	---	trace
1296	0.30	1.00	---	trace
1530	0.30	1.00	---	trace

* Includes appx. 0.5 wt% of β-$CaCr_2O_4$ (JCPDS-ICDD #9-146).

Table 2. Results of XRD analyses of $La_{0.7}Ca_{0.31}CrO_3$ samples heated at 2°C/min in air to peak temperature, then quenched.

Peak Temp.°C	Ca Concentration in Perovskite Phase (x)	Mole Fraction $La_{1-x}Ca_xCrO_3$ Phase	Mole Fraction $CaCrO_4$ Phase	Mole Frac. X-Ray Amorphous Phase
800	0.08	0.75	0.13	0.12
926	0.13	0.79	0.11	0.10
1015	0.17	0.84	0.08	0.09
1067	0.18	0.85	0.05	0.09
1126	0.20	0.87	0.04	0.09
1207	0.31	1.00	---	trace
1296	0.31	1.00	---	trace
1530	0.31	1.00	---	trace

During sintering, both LCC31 and LCC29 materials underwent roughly a 2% weight loss, after having been vacuum dried at 200°C for 2 hours. Presumably, the 2% loss is primarily due to evolution of oxygen as Cr^{+6} is reduced to Cr^{+4}. If all the non-perovskite material existed as $CaCrO_4$, then the reduction reaction could be written:

$$(1-q)La_{1-x}Ca_xCr^{+3}_{1-x}Cr^{+4}_xO_3 + qCaCr^{+6}O_4 \Rightarrow La_{0.7}Ca_{0.3}Cr^{+3}_{0.7}Cr^{+4}_{0.3}O_3 + q/2O_2\uparrow$$

In this case, a 2% weight loss due to oxygen would imply that roughly 25 mole% of the material existed as $CaCrO_4$ prior to weight loss ($q \approx 0.25$). Note that the LCC29 and LCC31 samples quenched from 800°C did contain roughly 25 and 21 mole% of phases other than the perovskite, respectively (Tables 1 and 2). This indicates that most of the Cr in the X-ray amorphous material is probably hexavalent at 800°C.

Weight loss curves, determined by thermogravimetric analysis, are plotted with the respective sintering shrinkage curves for LCC29 and LCC31 in Figures 8 and 9. The vertical scales are adjusted to emphasize the correlation of weight loss with densification events. In the case of LCC29, Figure 8, the weight loss ends near 1170°C. In contrast, the weight loss of LCC31, Figure 9, is correlated with the first rapid-shrinkage event, ending near 1100°C. This implies that all of the Cr^{+6} has been reduced to Cr^{+4} in the LCC31 material prior to the second rapid-shrinkage event.

4. DISCUSSION

a. Phase Changes and Sintering

The binary phase diagram between Ca and Cr oxides in air is relevant to the transitory conditions involved in chromite densification because the non-perovskite material is mainly composed of these two components. The most recent version of this diagram is published by Adendorff et al [16] from de Villiers et al [17]. This diagram shows a eutectic on the Ca-rich side of $CaCrO_4$ (Ca/Cr= 0.55/0.45, atom basis) at 1061°C. As discussed above, the X-ray amorphous portion of LCC31 probably has a Ca/Cr ratio near that of the eutectic and thus could be expected to melt almost completely by 1150°C. Therefore, it seems plausible that the second densification event in LCC31, near 1150°C, is due to liquid-phase sintering. In contrast, the X-ray amorphous portion of LCC29 probably has a Ca/Cr ratio that places it in the "β-$CaCr_2O_4$ + liquid" phase region at 1150°C, as indicated by the detection of β-$CaCr_2O_4$ along with $CaCrO_4$ at 1067°C. Therefore, the non-perovskite material in LCC29 might be expected to melt incongruently, retaining substantial solid phase at 1150°C. Nevertheless, *both* materials could be expected to form some liquid phase near 1061°C.

It is well known that A-site enriched chromites contain liquid-phase

remnants after sintering, but evidence of liquid formation has not been reported in A-site depleted samples, although these have been found to contain isolated Cr-rich deposits [5,7,11]. However, an LCC29 sample quenched from 1400°C contained isolated Cr-rich inclusions which, upon examination by SEM in polished cross section, were found to consist of rounded perovskite-like grains embedded in a matrix of essentially pure Cr oxide. This matrix phase may be a liquid-phase remnant that was progressively isolated and enriched in Cr as most of the original liquid was dissolved into the perovskite.

This leaves the problem of explaining why the LCC29 material does not densify even though a liquid phase is formed. In the case of LCC31, Figure 7 indicates that densification may not result directly from liquid formation, but rather from the subsequent dissolution of the liquid into the perovskite. This might indicate that the liquid does not adequately wet the solid perovskite in LCC31 until dissolution begins [18]. However, substantial Ca dissolution also takes place in the LCC29 material within the same temperature range; why does this not also lead to densification? The simple answer might be that liquid does not form in the LCC29 material, even though the present XRD analysis and the binary phase diagram indicate that it should.

It has been proposed that vapor-phase transport plays a role in preventing densification of the A-site depleted materials, such as LCC29 [1,5]. Yokokawa et al [1] argue that the presence of minor quantities of Cr_2O_3 will substantially increase the vapor pressure of CrO_3, causing vapor-phase transport and formation of Cr_2O_3 at intergranular necks, thus preventing further densification. This theory is supported by the work of Meadowcroft and Wimmer [19], whose data indicate that pure Cr_2O_3 vaporizes at a much higher rate than does $LaCrO_3$. However, it seems that the formation of a wetting liquid phase would overcome the effects of vapor-phase transport. Therefore, although vapor-phase transport may take place in samples that do not densify, it seems most likely that the *cause* of the lack of densification is the absence of an effective liquid phase. For example, in co-sintering studies, when the liquid phase in A-site enriched chromites has wicked into adjacent materials, the chromite does not densify [20]. In any case, although the empirical differences between Ca-enriched and Ca-depleted chromite sintering have been established, the basic mechanistic differences are not yet understood.

b. Effect of Powder Synthesis

The sintered densities obtained in the present study are similar to those obtained by Mori and co-workers [8], as shown in Figure 10, which compares the data for $La_{0.7}Ca_{0.32}CrO_3$ (LCC32). It should be noted, however, that the glycine-nitrate synthesized samples (present study) started at lower density at 1100°C, but attained high density (over 90%TD) by 1300°C as opposed to 1400°C for the Mori et al samples. These differences are attributed to the effects of powder synthesis and processing. Mori et al synthesized their chromite powders by co-precipitation followed by repeated calcination at 1000°C and ball milling.

Although no data are given, this procedure probably yields powders that have substantially larger particle size and higher dry-pressed green density than those produced for the present study by the glycine-nitrate process. Higher green density would result in higher sintered density at 1100°C. However, based on the data above 1200°C, it is apparent that the glycine-nitrate powder is more active.

The shrinkage curve for LCC31, shown in Figure 2, should be compared to the curve for a similar composition, $La_{0.7}Ca_{0.3}Cr_{0.98}O_3$, published by Sakai et al [7] in their Figure 2, which also exhibits two shrinkage events, but does not reach full density until about 1300°C. Sakai et al discussed three powder synthesis methods, the "ceramic," oxalic salt, and Pechini methods, although they do not specify which of the three was used for the dilatometer specimen, nor do they specify the calcination temperature; these ranged from 900° to 1100°C. They conclude that sinterability is independent of powder synthesis method and calcination temperature (see their Figure 1), but that improvement of sample homogeneity by increased milling results in higher sintered density (see their Table 1). However, it is apparent that glycine-nitrate synthesized powders reach high density at lower temperatures than do these less active powders. As shown in Table 3, glycine-nitrate powder, calcined at 900°C, attained 98.5%TD after sintering for 5 hr at 1250°C. Compare this to 92.5%TD, reported by Sakai et al for powder that was milled for 130 hr and sintered for 5 hr at 1300°C.

In the glycine-nitrate process, the precursor solution, in which the cations are intimately mixed on the molecular scale, is very rapidly transformed into oxide particles. For the chromites, the formation temperature of the powder (flame temperature) is near 1500°C [13]. At this temperature, the perovskite is stable at high Ca content. As the ash is heated during calcination and/or sintering, the non-perovskite phases, including $CaCrO_4$, are *exsoluted* from the perovskite. This exsolution takes place below 650°C, when the average perovskite crystallite size is still near 40 nm, assuring that the perovskite and non-perovskite phases are well mixed on a nano-scale. Subsequent growth of the particles to near 100 nm by 2 hr calcination at 900°C apparently does not result in significant demixing of the glycine-nitrate powder because high sintered density is still attained. The advantage of the 900°C calcination is that the green density is substantially increased, thereby reducing warpage during sintering.

Table 3. Results for sintering of glycine-nitrate synthesized $La_{0.7}Ca_{0.31}CrO_3$.

Calcination Conditions	Green Density % of Theoretical 6.085 g/cm^3=100%	Sintered Density 1250°C, 5 hr % of Theoretical 6.085 g/cm^3=100%
650°C 0.5 hr	37.0 n=1	98.1 n=2
900°C 2 hr	54.8 ±0.8 n=3	98.5 ±0.2 n=6

5. CONCLUSIONS

The main objective of this paper was to clarify the differences in phase changes and sintering between A-site enriched and A-site depleted chromites. It was established that A-site enriched $Y(Ca)CrO_3$ and $La(Ca)CrO_3$ sinter to high density below 1300°C in two rapid-shrinkage stages, whereas their A-site depleted counterparts only exhibit the first of these rapid-shrinkage events and do not reach high density. Phase changes are similar between A-site depleted and A-site enriched materials; over half of the Ca has been exsoluted into non-perovskite phases by the onset of sintering, and this Ca, along with associated Cr, dissolves back into the perovskite phase during sintering. XRD analysis implies that the non-perovskite phases should melt almost completely prior to the second rapid-shrinkage event in the A-site enriched samples, and should melt partially in the A-site depleted material.

Another purpose was to establish that the chromite powder synthesis method is an important variable even for A-site enriched chromites. In this regard, it was shown that glycine-nitrate synthesized $La_{0.7}Ca_{0.31}CrO_3$, with no milling, sinters to 98.5%TD in air at 1250°C, a substantial improvement over the performance of powders synthesized by other methods. The improved activity is attributed to small particle size and nano-scale mixing of phases.

6. ACKNOWLEDGEMENTS

The authors wish to thank JJ Kingsley for helpful suggestions and JL Aurand, TA Challman, and JP Lloyd for technical assistance.

7. REFERENCES

1. H Yokokawa, N Sakai, T Kawada, and M Dokiya, J. Electrochem. Soc. 138 [4] (1991) 1018-27.
2. M Dokiya, N Sakai, T Kawada, H Yokokawa, T Iwata and M Mori, in Proceedings of the First International Symposium on Solid Oxide Fuel Cells, ed. by SC Singhal. Electrochemical Society, Pennington, NJ. (1989) 325 -336.
3. N Sakai, T Kawada, H Yokokawa, and M Dokiya, J. Mat. Sci. 25 (1990) 4531.
4. N Sakai, T Kawada, H Yokokawa, M Dokiya and T Iwata, Solid State Ionics 40/41 (1990) 394-397.
5. LA Chick, JL Bates and GD Maupin, in Proceedings Second International Symposium on Solid Oxide Fuel Cells, ed. by F Grosz, P Zegers, SC Singhal and O Yamamoto, EUR 13564. Athens Greece. Commission of the European Communities, Luxembourg. (1991) 621-628.
6. H Yokokawa,N Sakai, T Kawada, and M Dokiya, *ibid.*, 663-670.
7. N Sakai, T Kawada, H Yokokawa, and M Dokiya, *ibid.*, 629-636.
8. M Mori, N Sakai, T Kawada, H Yokokawa, and M Dokiya, Denaki Kagaku 59 [4] (1991) 314-319.

9. JL Bates, LA Chick and WJ Weber, Solid State Ionics 52, (1992) 235-242.
10. H Yokokawa,N Sakai, T Kawada, and M Dokiya, *ibid.*, 43-56.
11. T Kawada, N Sakai, H Yokokawa, M Dokiya and I Anzai, Solid State Ionics 50 (1992) 189-196.
12. LA Chick, GD Maupin and JL Bates, in Proceedings of the Fifth Annual Conference on Fossil Energy Materials, Oak Ridge, TN, May 2, 1992 (in press).
13. Chick, LA, LR Pederson, GD Maupin, JL Bates, LE Thomas, and GJ Exarhos, Mater. Lett. 10 [1,2] (1990) 6-12.
14. LA Chick, GD Maupin, GL Graff, LR Pederson, DE McCready and JL Bates, in Synthesis and Processing of Ceramics: Scientific Issues, ed. by WE Rhine, TM Shaw, RJ Gottschall and Y Chen. Materials Research Society, 249 (1992) 159-164.
15. R Berjoan, C Romand and JP Coutures, High Temp. Sci. 13 (1980) 173-188.
16. KT Adendorff, JPR de Villiers and GJ Kruger, J. Am. Ceram. Soc. 75 [6] (1992) 1416-22.
17. JPR de Villiers J Mathias and A Muan, Trans. Inst. Metall. Sect. C, 96 (1987) C55-C62.
18. IA Aksay, CE Hoge and JA Pask, J. Phys. Chem. 78 [12] (1974) 1178-1183.
19. DB Meadowcroft and JM Wimmer, Bull. Am. Ceram. Soc. 58 (1979) 610-615.
20. TR Armstrong, LA Chick and JL Bates, in Proceedings of the Third International Symposium on Solid Oxide Fuel Cells, ed. by SC Singhal. The Electrochemical Society, Pennington, NJ. (1993).

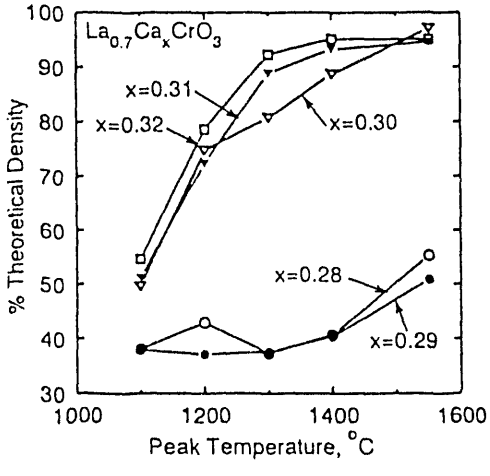

Figure 1. Sintered density versus peak temperature for $La_{0.7}Ca_xCrO_3$ samples heated at 1.6°C/min to peak temperature, then air quenched. 100% TD=6.085 g/cm^3.

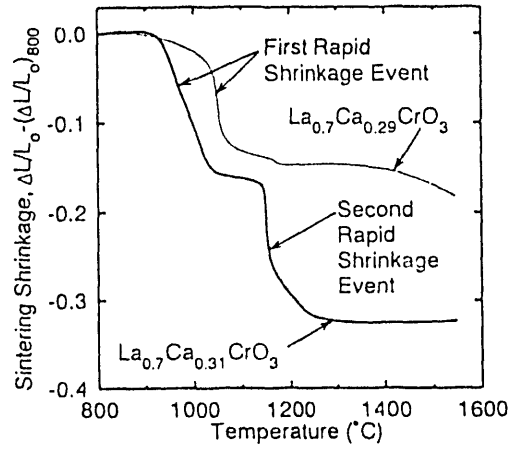

Figure 2. Sintering shrinkage curves for $La_{0.7}Ca_{0.29}CrO_3$ and $La_{0.7}Ca_{0.31}CrO_3$, measured on a vertical pushrod dilatometer heated at 2°C/min. Shrinkages set to zero at 800°C for comparison.

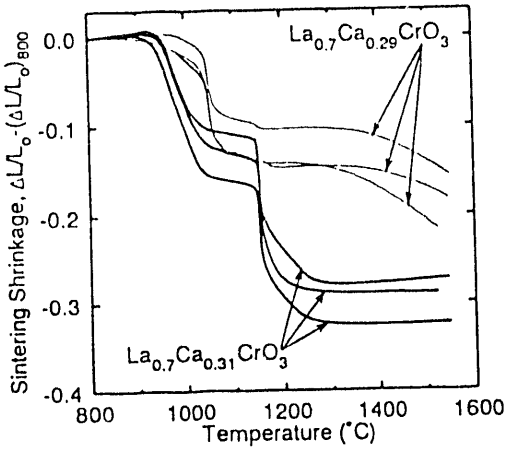

Figure 3. Sintering shrinkage curves for three replications each of $La_{0.7}Ca_{0.29}CrO_3$ and $La_{0.7}Ca_{0.31}CrO_3$, measured as in Figure 2. Each replication involved synthesizing a new batch of chromite powder.

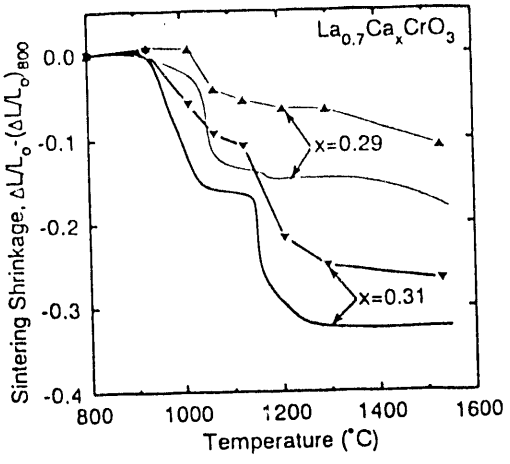

Figure 5. Triangular symbols are sintering shrinkages of $La_{0.7}Ca_{0.29}CrO_3$ and $La_{0.7}Ca_{0.31}CrO_3$ samples that were heated at 2°C/min, then quenched from peak temperature. Linear shrinkage was determined from immersion densities. Lines without symbols are dilatometer data from Figure 2.

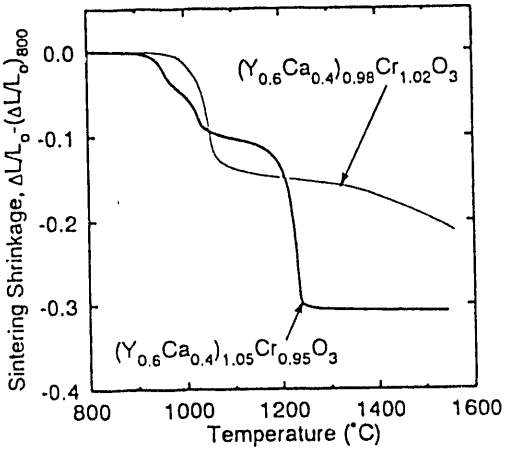

Figure 4. Sintering shrinkage curves for $(Y_{0.6}Ca_{0.4})_{0.98}Cr_{1.02}O_3$ and $(Y_{0.6}Ca_{0.4})_{1.05}Cr_{0.95}O_3$ measured as in Figure 2.

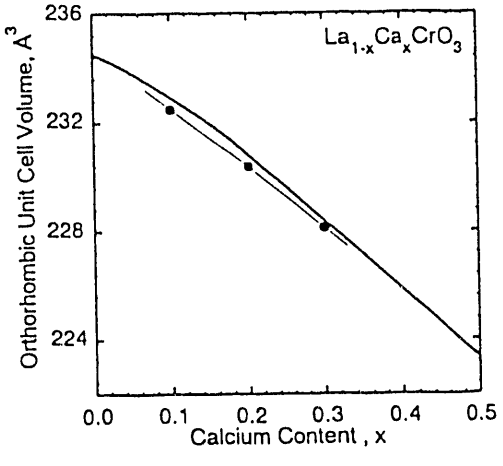

Figure 6. Relationship between orthorhombic unit cell volume and fraction of Ca in the perovskite, $La_{1-x}Ca_xCrO_3$. Bold line calculated from data in reference 15. Circular data points from this study, by XRD on samples heated at 1500°C, 2hr.

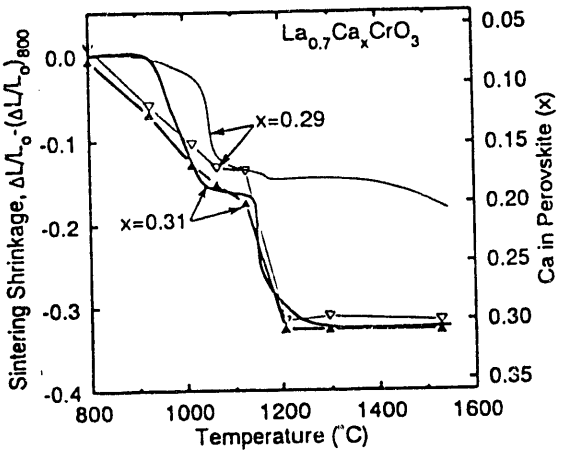

Figure 7. Triangular symbols are estimated levels of Ca in the perovskite phase of samples shown in Figure 5, calculated from thin line in Figure 6. Lines without symbols are dilatometer data from Figure 2.

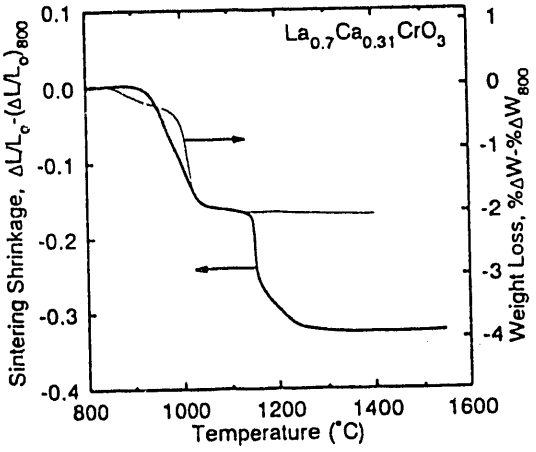

Figure 9. Thermogravimetric weight loss curve for $La_{0.7}Ca_{0.31}CrO_3$ (thin line) heated at 2°C/min. Bold line is dilatometry data for the same composition, from Figure 2.

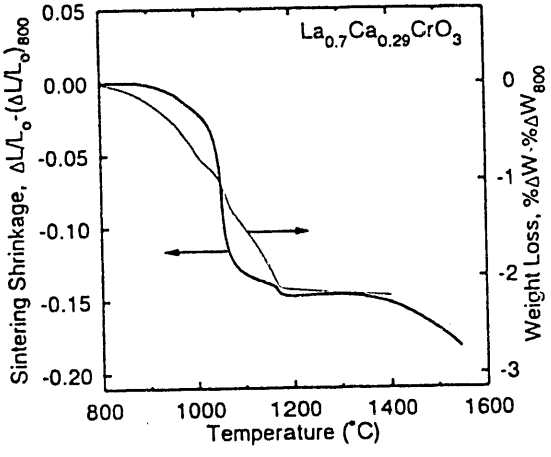

Figure 8. Thermogravimetric weight loss curve for $La_{0.7}Ca_{0.29}CrO_3$ (thin line) heated at 2°C/min. Bold line is dilatometry data for the same composition, from Figure 2.

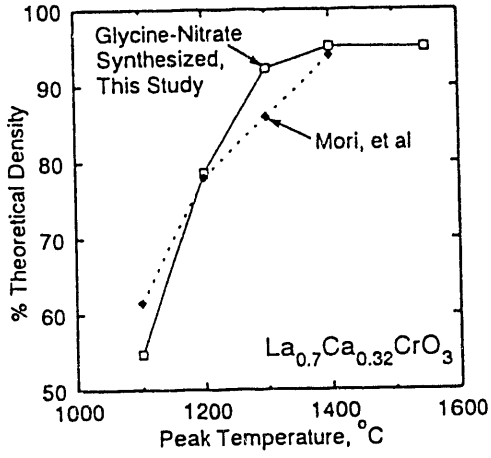

Figure 10. Comparison of sintered densities for $La_{0.7}Ca_{0.32}CrO_3$. Open squares are for material synthesized by glycine-nitrate process, from Figure 1. Filled squares are data from Mori et al [8].

DATE
FILMED
8/30/93

END